# Mode III interlaminar fracture of carbon/epoxy laminates using the edge crack torsion (ECT) test

A.B. de Morais, A.B. Pereira, M.F.S.F. de Moura, A.G. Magalhães

A B S T R A C T

The mode III interlaminar fracture of carbon/epoxy laminates was evaluated with the edge crack torsion (ECT) test. Three-dimensional finite element analyses were performed in order to select two specimen geometries and an experimental data reduction scheme. Test results showed considerable non-linearity before the maximum load point and a significant *R*-curve effect. These features prevented an accurate definition of the initiation point. Nevertheless, analyses of non-linearity zones showed two likely initiation points corresponding to $G_{IIIc}$ values between 850 and 1100 J/m$^2$ for both specimen geometries. Although any of these values is realistic, the range is too broad, thus showing the limitations of the ECT test and the need for further research.

*Keywords:*

A. Polymer–matrix composites (PMCs)
B. Fracture toughness
B. Delamination
C. Finite element analysis (FEA)
Mode III

## 1. Introduction

Delamination in high performance composites has been subject of research for many years [1,2]. In fact, this failure mode is particularly insidious as it may escape detection and yet cause dramatic losses of structural performance. Fracture mechanics principles and tools have proved to be the most adequate for analysis of delamination problems. Therefore, characterisation of delamination resistance under the basic loading modes is needed. Compared to mode I and mode II fracture, much less work has been reported on mode III [1,2], despite its importance in edge delamination [3,4]. The split cantilever beam (SCB) [5] was one of the first tests used to measure the mode III critical strain energy release rate $G_{IIIc}$. However, finite element (FE) analyses [6] showed the presence of a significant mode II component. Robinson and Song [7] modified the SCB test in order to eliminate the spurious mode II. However, the high stiffness of the SCB specimen prevents experimental compliance calibration, thus requiring accurate shear moduli [7]. The crack rail shear (CRS) test [8] has the same handicap.

In these circumstances, recent studies have focussed on the edge crack torsion (ECT, Fig. 1) test [1,2,9–17]. The original fixture [9] consisted of three support pins and an upper loading pin, which introduce the loads *Q* represented in Fig. 1. Such loads generate the torsion moments responsible for the mode III shear sliding. The specimen stacking sequence proposed by Lee [9] was $[90/(\pm 45)_n/(\mp 45)_n/90]_s$ with $n = 3$ or 4, so that the delamination propagates at mid-thickness between 90° plies. It should be noted that the 90° direction coincides with the *y*-direction of Fig. 1 and therefore the delaminating interface is equivalent to the standard 0/0 adopted for modes I and II tests [1,2]. However, ±45° plies are needed for torsional stiffness and strength.

Numerical analyses [12,13,16] of the ECT specimen showed there is some mode II near the edges. Suemasu [14] used end steel blocks instead of loading pins in order to obtain uniform pure mode III. Nevertheless, it is possible to minimise the spurious mode II by an appropriate choice of specimen geometry [13], e.g. $b = 38$ mm, $c = 76$ mm, $d = 32$ mm and $l = 89$ mm [12]. In fact, propagation was shown to occur in the specimen mid-region, which is under pure mode III [12,16]. More recently [16] the length $l$ (Fig. 1) was increased to 108 mm and the lay-up changed to $[90/0/(\pm 45)_n/(\mp 45)_n/0/90]_s$ for further reduction of the spurious mode II. Load application via both upper pins was also adopted to avoid geometric non-linearity [16].

Naturally, data reduction in ECT tests is more complex than in modes I and II fracture tests. The first analysis by Lee [9] applied the mechanics of materials moment-rotation relation to the delaminated and non-delaminated parts of the specimen, and used Classical Lamination Theory (CLT) to derive the torsional stiffness of each part. However, this analysis violates boundary conditions and does not take into account transverse shear. Li and O'Brien [10] incorporated the effect of transverse shear, but a numerical solution seems to be required for the formulation that satisfies boundary conditions [11]. Therefore, more recent experimental

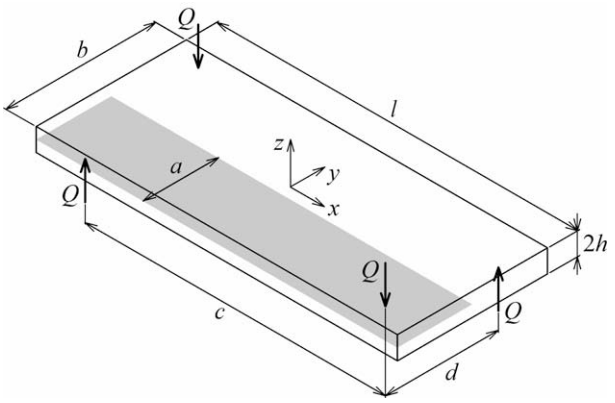


**Fig. 1.** The ECT specimen.

studies [12,15–17] have used a compliance calibration type method, which requires specimens with different crack lengths. In fact, the crack position cannot be monitored during ECT tests and the crack length cannot be varied by repositioning a single specimen. However, this method bears errors inherent to specimen variability and increases substantially test costs. Moreover, the basic compliance-crack length relation is similar to the one obtained by Lee [9]. Nevertheless, good fits have been reported in experimental studies [12,15,16].

Other problems may affect ECT tests, e.g. identifying correctly the initiation point. The commonly employed non-linearity and maximum load criteria [2] can give substantially different results, especially for glass-fibre composites [16,17]. This has been attributed to the formation of intraply cracks in interface 90° plies [15,16]. Significant crack length dependency of the perceived $G_{IIIc}$ is another problem in ECT tests [16,17].

Therefore, considerable research is still needed to validate the ECT test for measuring $G_{IIIc}$ of laminated composites. The present study aimed at evaluating its adequacy for a carbon/epoxy material by combining numerical analyses and experimental tests.

## 2. Analysis

The objective of this work was to measure initiation $G_{IIIc}$ values of specimens obtained from a UD high strength carbon fibre (T300)/toughened epoxy prepreg (reference HS 160 REM) supplied by Texipreg. The modes I and II fracture of UD specimens made from this material was investigated in [18], where average $G_{Ic} \approx 250$ J/m$^2$ and $G_{IIc} \approx 800$ J/m$^2$ were obtained. Ply elastic properties were previously determined: $E_1 = 130$ GPa, $E_2 = 8.2$ GPa, $\nu_{12} = 0.27$, $\mu_{12} = 4.1$ GPa, $\nu_{23} = 0.41$ and thickness $t = 0.15$ mm. In these circumstances, a preliminary selection of specimen lay-up and geometry was made considering the above literature review. Li et al. [12] reported consistent toughness values without transverse cracking problems for $[90/(\pm45)_3/(\mp45)_3/90]_s$ specimens with thickness $2h = 4.9$ mm. This stacking sequence is more effective in avoiding transverse cracks in interface 90° plies than the one used recently by Ratcliffe [16], since the incorporation of 0° plies reduces torsional stiffness and strength. Therefore, in view of the ply thickness of the present carbon/epoxy material, the stacking sequence used was $[90/(\pm45)_4/(\mp45)_4/90]_s$, resulting in nominal $2h = 5.4$ mm. On the other hand, the dimensions selected were (Fig. 1) $l = 96$ mm, $b = 40$ mm, $c = 80$ mm, $d = 30$ mm and crack lengths $a = 10$, 15, 20 and 25 mm in order to apply the compliance calibration (CC) [12]

$$\frac{1}{C} = A - ma \tag{1}$$

where $A$ and $m$ are determined by data fitting. The compliance is here defined as $C = \delta/P$ with $P = 2Q$ (Fig. 1), i.e. the loading was applied to both upper pins as in [16]. The Irwin–Kies relation then gives

$$G_{III} = \frac{mP^2}{2c(A - ma)^2} \tag{2}$$

assuming that all energy is released within the region delimited by the positions of the pins and that it is pure mode III. As mentioned above, Eq. (1) has the same form of the plate theory (PT) based expression derived by Lee [9], which predicts

$$A = \frac{32\mu_{xy,0}h^3b}{3cd^2},\ m = \frac{32\mu_{xy,0}h^3}{3cd^2}\left(1 - \frac{\mu_{xy,1}}{4\mu_{xy,0}}\right) \tag{3}$$

where $\mu_{xy,0}$ and $\mu_{xy,1}$ designate the CLT torsional shear moduli of the uncracked and cracked parts of the specimen, respectively.

The proposed specimen geometry and data reduction method were evaluated by three-dimensional (3D) FE analyses. The models were constructed with the ABAQUS® code using 8-node elements (Fig. 2). In most areas multi-ply elements were used in order to achieve accurate results without excessive computational cost. Nevertheless, the two plies of the delamination interface were modelled by individual layers of elements. Moreover, mesh refinement was done near the delamination tip and towards the edges, regions where displacement fields suffer more pronounced variations. This refinement allowed the calculation of accurate strain energy release rate components by the virtual crack closure technique (VCCT) [19]. The models included two upper loading and two lower support rigid spheres. Contact surfaces were defined at the faces of the elements of the starter delamination and of the areas under the influence of the spheres. Cinematic conditions were imposed on nodes of the elements under the action of the spheres in order to avoid local crushing. Therefore, specimen indentation by the spheres was not modelled, because this would require high levels of local mesh refinement and create unnecessary numerical convergence difficulties. In-plane ($xy$) rigid body motions were prevented by constraining lengthwise $u$ and widthwise $v$ displacements of three nodes on the mid-plane of the uncracked part of the specimen (Fig. 3). As in [16], it was verified that those constraints did not influence the results. In fact, they were removed after an initial loading step because the forces developed by contact with the spheres prevented rigid body motions.

The VCCT analysis showed that the proposed specimens are clearly mode III dominated (Fig. 4), as the mode II region is quite limited and has small $G_{II}$ peaks. The $a = 10$ mm specimen seemed satisfactory despite the mild $G_{III}$ peaks. Nevertheless, specimens with $a \geqslant 15$ mm have a significant mid-region of quasi-uniform $G_{III}$. However, the distribution of $G_{III}$ inside the area delimited by the pins positions ($c$ in Fig. 1) becomes clearly less uniform for $a = 25$ mm.

As for the above data reduction schemes, the CC method was able to fit quite well FE compliance results (Fig. 5). However, it failed to give consistent $G_{III}$ predictions for the whole range of specimen crack lengths (Fig. 6). In fact, the CC scheme may deviate considerably from both lengthwise average and maximum values. Moreover, it would lead to an increase of perceived $G_{IIIc}$ with the crack length. This was actually observed in [16,17], although the specimen lay-up and geometry used were somewhat different. On the other hand, as expected, Lee's [9] PT scheme underestimated significantly the specimen compliance (Fig. 5) and both lengthwise average and maximum $G_{III}$ values (Fig. 6). Therefore, neither of these data reduction schemes is satisfactory.

In view of the above results, another approach was pursued that is based on the analyses of Liao and Sun [11] and Suemasu [14] for

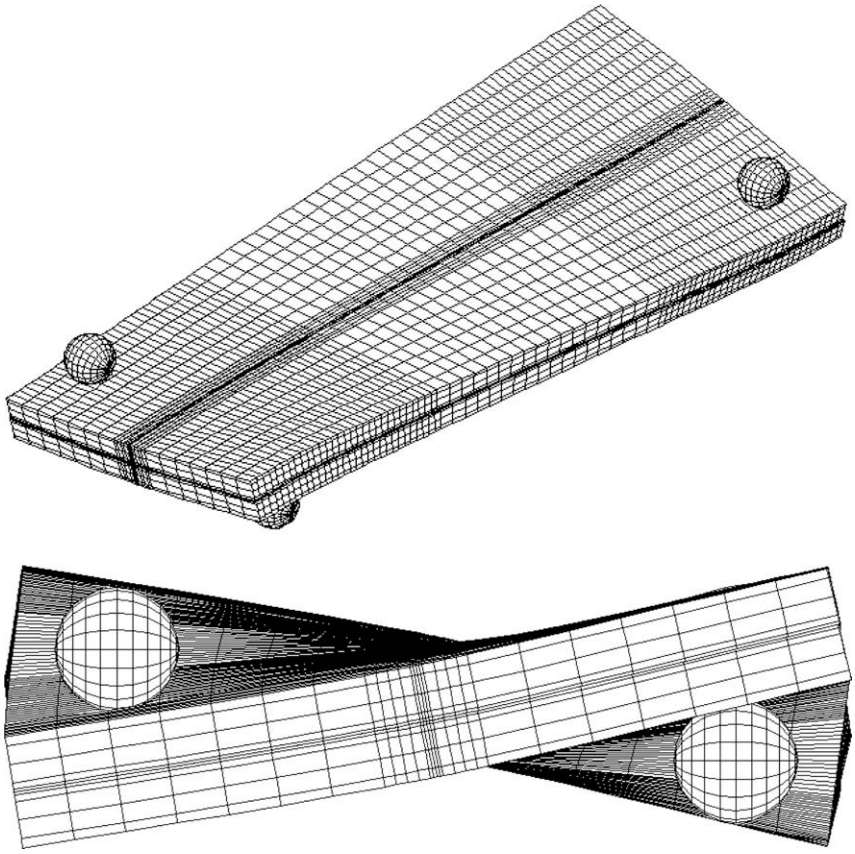

**Fig. 2.** FE model of an ECT specimen in the deformed configuration.

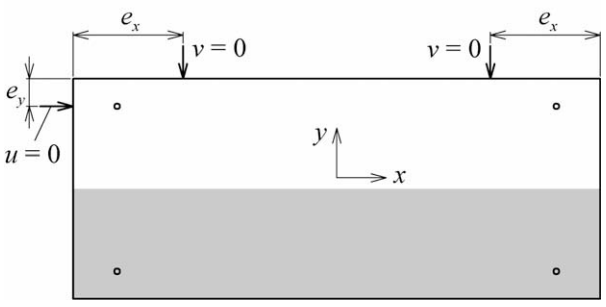


**Fig. 3.** Boundary conditions in the specimen mid-plane ($xy$). Edge distances $e_x$ = 10 mm and $e_y$ = 20 mm were used in the analyses.

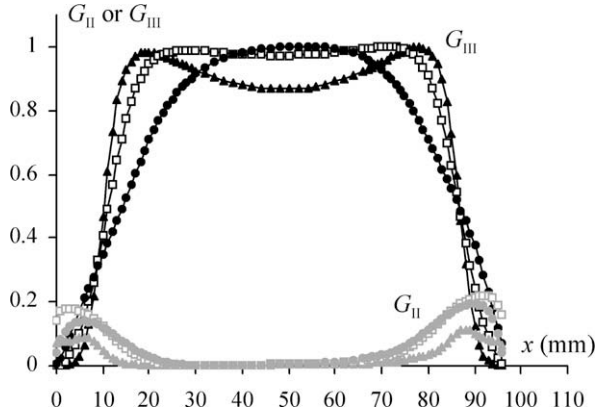


**Fig. 4.** Lengthwise distributions of $G_{II}$ and $G_{III}$ normalised by the maximum $G_{III}$ value for specimens with $a$ = 10 (▲,▲), 15 (□,□) and 25 mm (●,●).

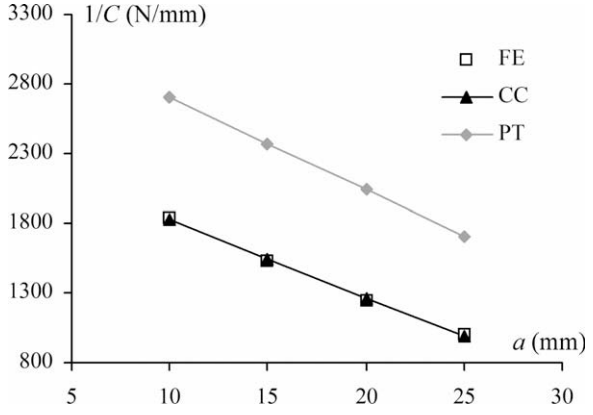


**Fig. 5.** Comparison of inverse compliance FE results with CC and PT predictions.

ECT specimens with $b = 2a$ (Fig. 1). Both analyses lead to closed-form expressions and assume $\mu_{xy,1} = \mu_{xy,0} = \mu_{xy}$, relations that are only exact for angle-ply lay-ups [11]. The relation between the torque $M = Qd$ and the rotation angle per unit length $\omega = 2\delta/cd$ (Fig. 1) is [11]

$$\frac{M}{\omega} = \mu_{xy}\left[\frac{4bh^3}{3} - \frac{256h^4}{\beta\pi^5}\sum_{n=1,3,5\ldots}^{\infty}\frac{1}{n^5}\tanh\left(\frac{\beta n\pi b}{2h}\right)\right] \tag{4}$$

where $\beta = (\mu_{xz}/\mu_{xy})^{1/2}$ and $\mu_{xz}$ is the through-thickness shear modulus. Therefore, in view of the typical specimen geometry and shear moduli

$$\frac{1}{C} \approx \frac{16h^3\mu_{xy}}{cd^2}\left(\frac{b}{3} - \frac{64h}{\beta\pi^5}\right) \tag{5}$$

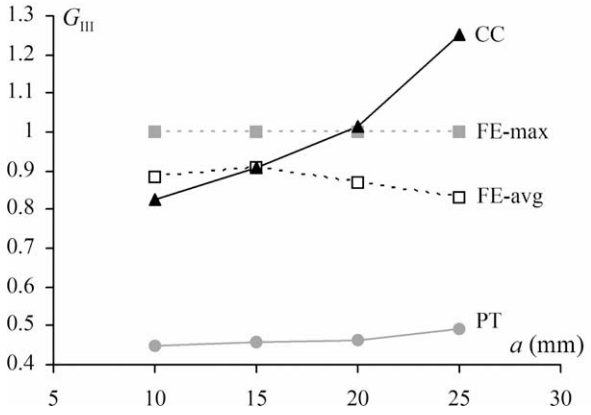


**Fig. 6.** Comparison of $G_{III}$ FE results with CC and PT predictions. All values were normalised by the maximum $G_{III}$ FE value.

On the other hand, Suemasu [14] showed that for pure torsion

$$G_{III} \approx \mu_{xy} h^3 \omega^2 \tag{6}$$

which can be expressed as

$$G_{III} \approx \frac{4\mu_{xy} h^3 \delta^2}{(cd)^2} \tag{7}$$

Although the point loadings used in the selected test setup do not ensure pure torsion in the whole specimen, this condition exists in the mid-region. The main problem in applying Eqs. (5) and (7) is the need of the $\mu_{xy}$ and $\mu_{xz}$ moduli. Using the nominal ply properties mentioned above, CLT torsional shear moduli of the selected specimens are $\mu_{xy,0} = 28.91$ and $\mu_{xy,1} = 24.26$ GPa, thus casting ambiguity over which $\mu_{xy}$ should be used. On the other hand, we obtain from [20] $\mu_{xz,0} = \mu_{xz,1} = 3.56$ GPa, showing that the transverse shear term will have a relatively small effect on specimen compliance (lower than 12%). In these circumstances, one can assume $\mu_{xz} = 3.56$ GPa without introducing significant errors, thus allowing $\mu_{xy}$ to be computed from Eq. (5).

Obviously, owing to the $b = 2a$ geometry assumed, this scheme can only be applied to the $a = 20$ mm specimen defined above. However, crack length dependent perceived $G_{IIIc}$ values have been reported [16,17] and thus a specimen with $a = 30$ mm and $b = 60$ mm was also considered. In principle, the specimen length $l$ (Fig. 1) should be much higher than the 96 mm used so far to ensure mode III dominance [11,13]. This would increase significantly the cost of the specimen and hence a different approach was adopted. It can be seen in Fig. 2 that the mode II component is associated to local bending, which is far more pronounced in the predelaminated part of the specimen, because of its much lower stiffness. Therefore, in the $a = 30$ mm and $b = 60$ mm specimen the support and load points acting on the delaminated region were placed at a larger distance from the edge, as shown in Fig. 7. The VCCT analyses confirmed the prevalence of mode III on this new specimen and a large $G_{III}$ plateau (Fig. 8). Application of the data reduction scheme outlined above gave $\mu_{xy} = 24.0$ and 27.5 GPa for the narrow ($b = 40$ mm) and wide ($b = 60$ mm) specimens, respectively. Errors of Eq. (7) relative to the maximum VCCT $G_{III}$ were −1.3 and −2.2%, which can be considered quite good. The effect of friction was also evaluated by adopting a 0.4 friction coefficient [21] for the contact between delaminated plies. Results showed friction effects on specimen compliance and energy release rates were lower than 0.3%, hence negligible.

Finally, crack growth simulations were also performed using the interface elements developed by de Moura and coworkers [22,23], which include a cohesive zone damage model. The model has been used to study crack initiation in modes I and II interlaminar fracture [24,25]. Its application to the proposed ECT specimens was done in identical terms and therefore model description is not repeated here. The variables inputted in the damage model were interlaminar strengths $\sigma_{u3} = \tau_{u13} = \tau_{u23} = 70$ MPa, and $G_{Ic} = 250$ J/m$^2$, $G_{IIc} = 800$ J/m$^2$ and $G_{IIIc} = 900$ J/m$^2$. The latter value will find some support in Section 3, but, at this stage, the main objective was to perform an additional evaluation of the proposed specimens and data reduction scheme. This implied comparing the inputted $G_{IIIc}$ with the value obtained from Eq. (7) using the initiation load $P_c$. It was also necessary to define an appropriate initiation criterion, i.e. the non-linearity or the maximum load. Fig. 9 shows the

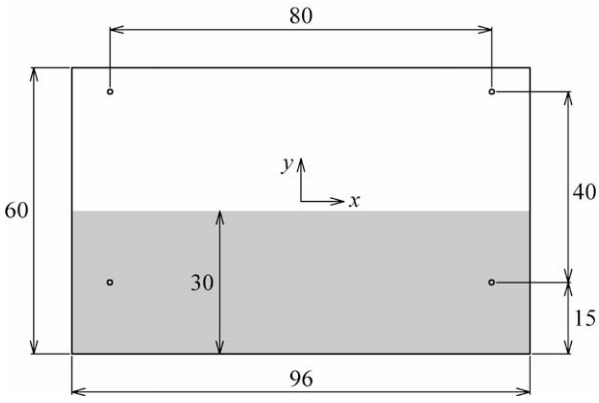


**Fig. 7.** Geometry of the wide specimen used in this work, including the positions of support and loading points (dimensions in mm).

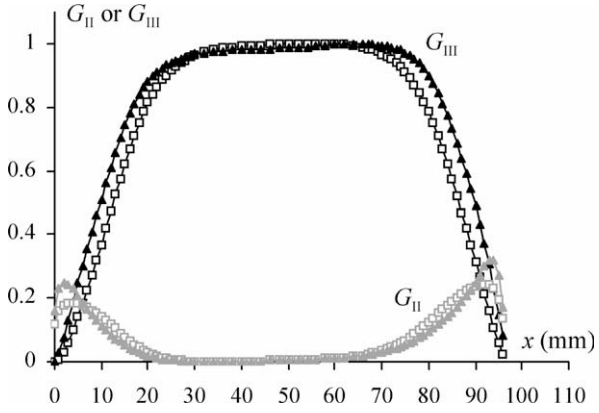


**Fig. 8.** Lengthwise distributions of $G_{II}$ and $G_{III}$ normalised by the maximum $G_{III}$ value for specimens with $a = 20$ (□,□) and 30 (▲,▲) mm.

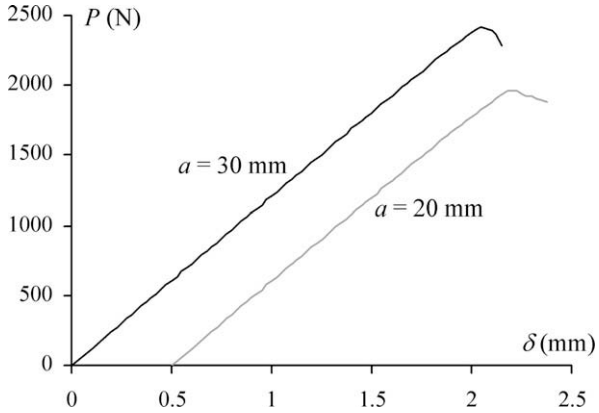


**Fig. 9.** Load displacement curves obtained in simulations with the cohesive zone damage model. For clarity, one curve was offset by 0.5 mm.

load–displacement curves obtained for the two specimens selected. Initiation occurred in the middle of the specimens at the maximum load point. Deviations from linearity at the latter point were 4.9% and 2.9% for the narrow and wide specimens, respectively. They can be attributed to the cohesive damage zone ahead of the crack tip [24,25]. $G_{IIIc}$ values obtained from Eq. (7) were 914 and 875 J/m$^2$ for the narrow and wide specimens, which correspond to 1.6% and −2.8% errors relative to the value inputted in the damage model. These results confirmed the adequacy of the approach proposed.

## 3. Experimental

Laminated plates were obtained from a UD high strength carbon fibre (T300)/toughened epoxy prepreg (reference HS 160 REM) supplied by Texipreg. A 13 μm thick PTFE film was inserted during lamination to generate the starter crack. Hot plate pressing was then conducted according to recommended processing conditions. Four specimens of each of the above geometries were cut from the plates. The test fixture employed followed the design adopted in [16] (Fig. 10) with two upper loading pins connected to a rigid frame attached to the load cell. Loading and support pins had 6 mm diameter hemispherical ends. As in [12,16], three guide-pins were used in the positions given in Fig. 3 for specimen alignment and to prevent initial rigid body motions. The guide-pins were removed after a small initial preload. Tests were performed on a Shimadzu machine at 1 mm/min crosshead speed. The compliance of the loading system (fixture and machine) and specimen indentation was measured using remaining non-delaminated parts of the plates. Specimen compliances were subsequently discounted of the loading system and indentation compliance.

Fig. 11 shows typical loading displacement curves, where considerable non-linearity before the maximum load is clearly noticeable. The non-linearity was more pronounced in narrow specimens, as predicted by the damage simulation FE analysis. However, non-linearity levels are much higher than those obtained in FE simulations. As seen in Section 1, one of the possible explanations was transverse cracking of the interface 90° plies [16]. However, FE simulations employing very low transverse properties for 90° interface plies showed that such cracks could not promote the observed non-linearity levels. Moreover, X-radiographs performed in a Satelec DG-073B machine did not reveal any transverse cracks. Specimens were then cut along the mid-section and optical microscope observation of the cross-sections confirmed delamination growth, as exemplified in Fig. 12. Therefore, the pronounced non-linearity resulted from delamination growth with an *R*-curve ef-

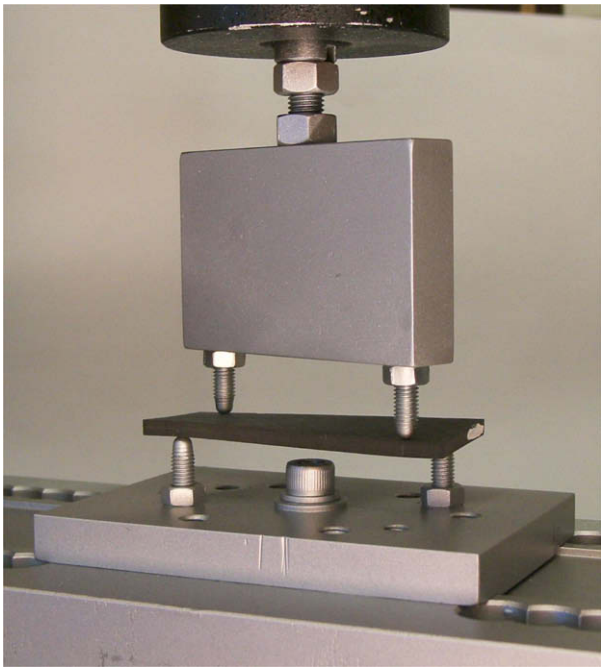

**Fig. 10.** Picture of the test rig.

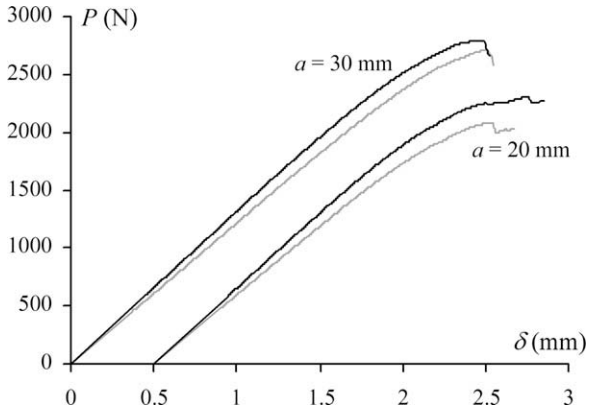


**Fig. 11.** Typical experimental load–displacement curves. For clarity, curves for narrow specimens were offset by 0.5 mm.

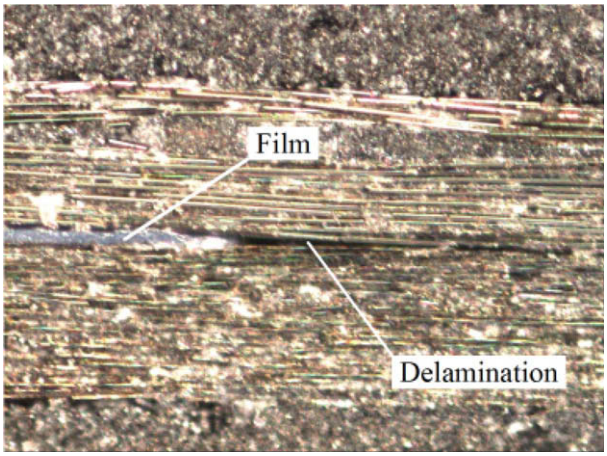


**Fig. 12.** Optical microscope picture of the mid-section of a tested specimen.

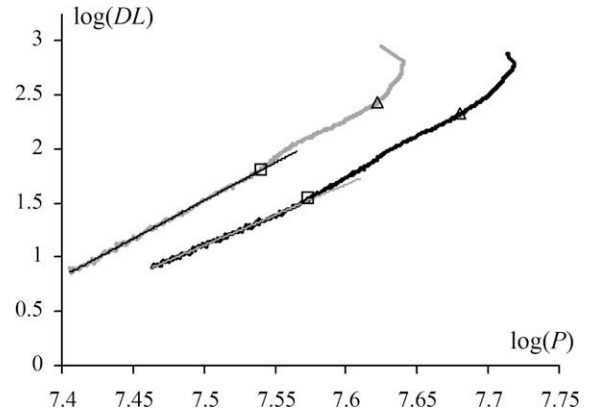


**Fig. 13.** Definition of non-linearity initiation points in two narrow specimens. Line fits to the initial parts of the curves are included.

fect. If we define the deviation from linearity ($DL$) in terms of percent increase of compliance, i.e. $DL = (C - C_0)/C_0$, an initial linear $\log(DL) - \log(P)$ variation can be seen in all specimens (Figs. 13 and 14). Such initial deviations from linearity are surely associated to the formation of the fracture process zone. Consequently, we can define a first non-linearity initiation point, hereafter designated as NL1, which corresponded to $DL = 4.7$–$6.2\%$ in narrow specimens and to $DL = 3.3$–$4.9\%$ in wide ones. The $\log(DL) - \log(P)$ curves (Figs. 13 and 14) also show a second region of non-linearity, where the variation was practically linear in wide specimens. A second initiation point (NL2) was defined at the end of this region, which corresponded to $DL = 10.0$–$12.6\%$ in narrow specimens and to $DL = 5.1$–$9.3\%$ in wide ones.

Finally, the above data reduction scheme was applied. Fig. 15 shows the shear moduli $\mu_{xy}$ calculated from the specimen initial compliance and Eq. (5). It can be seen that they agree quite well with FE values, thus giving confidence in the approach adopted. On the other hand, initiation points that resulted from the analysis of load–displacement curves gave very similar $G_{IIIc}$ values for both specimen geometries (Fig. 16). The scatter (8.6% maximum standard deviation) is comparable to the commonly observed in mode II fracture tests. Furthermore, any of the initiation points gives realistic $G_{IIIc}$ values, as they are believed to be higher than $G_{IIc}$. In fact, average $G_{IIc} \approx 800\ \mathrm{J/m^2}$ were obtained in previous work [18]. However, the 850–1100 J/m$^2$ interval does not enable a satisfactory characterisation of the initiation $G_{IIIc}$. This is not surprising, as the problem of defining crack initiation has not been completely solved in modes I and II interlaminar fracture tests. Moreover, the ECT is clearly a more complicated test, since crack propagation cannot be followed and results indicate an $R$-curve effect. Therefore, further research on mode III fracture is needed, including the possible development of alternative test methods.

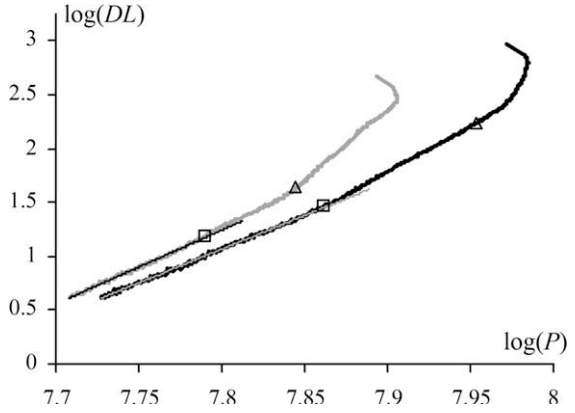


**Fig. 14.** Definition of non-linearity initiation points in two wide specimens. Line fits to the initial parts of the curves are included.

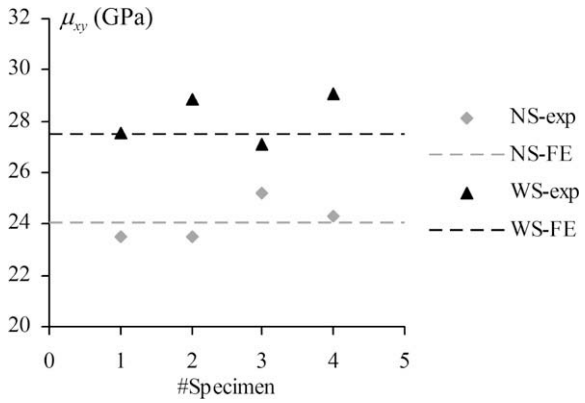


**Fig. 15.** Experimental shear moduli and FE model predictions for narrow (NS) and wide (WS) specimens.

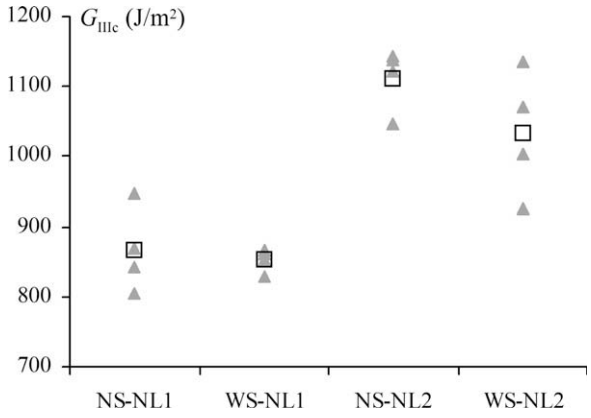


**Fig. 16.** Toughness values obtained for narrow (NS) and wide (WS) specimens with the two initiation criteria (NL1 and NL2) adopted. Specimen data (▲) and average (□) values are depicted.

## 4. Conclusions

The mode III interlaminar fracture of carbon/epoxy laminates was investigated with the edge crack torsion (ECT) test. Preliminary three-dimensional finite element analyses were conducted to evaluate the usual approach that consists in using specimens with different crack lengths and employing a compliance calibration scheme. The results showed that such scheme yields significant errors in the mode III strain energy release rate $G_{III}$. Plate theory based analyses also proved to be inappropriate. Therefore, an alternative method was used, based on the analyses of Liao and Sun [11] and Suemasu [14]. This required selecting specimens with a starter delamination equal to half-width, including a novel geometry with widthwise asymmetric positions for the loading pins.

Predicted specimen compliances were in good agreement with experimental values. However, there was considerable non-linearity before the maximum load point associated with an $R$-curve effect. This prevented an accurate definition of the initiation point. Nevertheless, analyses of load–displacement curves showed two main stages of non-linearity, which allowed the definition of two initiation points. These corresponded to $G_{IIIc}$ values between 850 and 1100 J/m$^2$ for both specimen geometries, which can be considered realistic in view of the previously measured $G_{IIc}$ around 800 J/m$^2$. Although uncertainty remains over the exact definition of initiation in other interlaminar fracture tests, the range of $G_{IIIc}$ values is clearly too broad. Therefore, further research on mode III fracture is needed, including the possible development of alternative test methods.

## Acknowledgments

This work was performed for the POCI/EME/57956/2004 research project, which is supported by the Portuguese Foundation for Science and Technology (FCT) and by the FEDER European Union fund. The authors thank the collaboration of Professor A.T. Marques (FEUP, Portugal) and C. Novo (INEGI, Portugal).

## References

[1] Tay TE. Characterization and analysis of delamination fracture in composites: an overview of developments from 1990 to 2001. Appl Mech Rev 2003;56:1–31.
[2] Brunner AJ, Blackman BRK, Davies P. A status report on delamination resistance testing of polymer–matrix composites. Eng Fract Mech 2008;75:2779–94.

[3] O'Brien TK, Raju IS. Strain energy release rate analysis of delamination around an open hole in composite materials. In: 25th AIAA/ASME/ASCE/AHS structures, structural dynamics and materials conference, Palm Springs, CA; 1984. p. 526–36.
[4] Wang SS. Fracture mechanics for delamination problems in composite materials. J Compos Mater 1983;17:210–33.
[5] Donaldson SL. Mode III interlaminar fracture characterization of composite materials. Compos Sci Technol 1988;32:225–49.
[6] Martin RH. Evaluation of the split cantilever beam for mode III interlaminar delamination testing. In: O'Brien TK, editor. ASTM STP 1110, Composite materials: fatigue and fracture, vol. 3. Philadelphia (PA): American Society for Testing and Materials; 1991. p. 243–66.
[7] Robinson P, Song DQ. The development of an improved mode III delamination test for composites. Compos Sci Technol 1994;52:217–33.
[8] Becht G, Gillespie JW. Design and analysis of the Cracked Rail Shear specimen for mode III interlaminar fracture. Compos Sci Technol 1988;31:143–57.
[9] Lee SM. An edge crack torsion method for mode III delamination fracture testing. J Compos Technol Res 1993;15:193–201.
[10] Li J, O'Brien TK. Simplified data reduction methods for the ECT test for mode III interlaminar fracture toughness. J Compos Technol Res 1996;18:96–101.
[11] Liao WC, Sun CT. The determination of mode III fracture toughness in thick composite laminates. Compos Sci Technol 1996;56:489–99.
[12] Li J, Lee SM, Lee EW, ÓBrien TK. Evaluation of the edge crack torsion (ECT) test for mode III interlaminar fracture toughness of laminated composites. J Compos Technol Res 1997;19:174–83.
[13] Zhao D, Wang Y. Mode III fracture behaviour of laminated composite with edge crack in torsion. Theor Appl Fract Mech 1998;29:109–23.
[14] Suemasu H. An experimental method to measure the mode III interlaminar fracture toughness of composite laminates. Compos Sci Technol 1999;59:1015–21.
[15] Li X, Carlsson LA, Davies P. Influence of fiber volume fraction on mode III interlaminar fracture toughness of glass/epoxy composites. Compos Sci Technol 2004;64:1279–86.
[16] Ratcliffe JG. Characterization of the edge crack torsion (ECT) test for mode III fracture toughness measurement of laminated composites. NASA/TM-2004-213269.
[17] Pennas D, Cantwell WJ. The influence of strain rate on the mode III interlaminar fracture of composite materials. J Compos Mater 2007;41:2595–614.
[18] de Morais AB, Pereira AB. Application of the effective crack method to mode I and mode II interlaminar fracture of carbon/epoxy unidirectional laminates. Compos Part A 2007;38:785–94.
[19] Krueger R. The virtual crack-closure technique: history, approach and applications. ICASE report 2002-10. NASA/CR-2002-211628.
[20] Sun CT, Li S. Three-dimensional effective elastic constants for thick laminates. J Compos Mater 1988;22:629–39.
[21] Davidson BD, Sun X. Effects of friction, geometry, and fixture compliance on the perceived toughness from three- and four-point bend end-notched flexure tests. J Reinf Plast Compos 2005;24:1611–28.
[22] de Moura MFSF, Gonçalves JPM, Marques AT, Castro PMST. Modeling compression failure after low velocity impact on laminated composites using interface elements. J Compos Mater 1997;31:1462–79.
[23] Gonçalves JPM, de Moura MFSF, Castro PMST, Marques AT. Interface element including point-to-surface constraints for three dimensional problems with damage propagation. Eng Comput 2000;17:28–47.
[24] de Morais AB, de Moura MFSF. Assessment of initiation criteria used in interlaminar fracture tests of composites. Eng Fract Mech 2005;72:2615–27.
[25] de Morais AB, de Moura MFSF. Evaluation of initiation criteria used in interlaminar fracture tests. Eng Fract Mech 2006;73:2264–76.